Environmental Pollution 386 (2025) 127163

Contents lists available at ScienceDirect

Environmental Pollution

journal homepage: www.elsevier.com/locate/envpol

Impacts of soil humic acids on the presence of PPCPs in reclaimed water☆

J.E. Conde-González [a], Hernández Z [b,c], Aguiar V [a], Vera L [d], Marrero MC [d], Salvadó V [e], Peña-Méndez EM [a,*]

[a] Departamento de Química, Unidad Departamental de Química Analítica, Facultad de Ciencias, Universidad de La Laguna, Avda. Astrofísico Fco. Sánchez, s/n, 38206 La Laguna, Spain
[b] UAM Copernicus Laboratory, Universidad Autónoma de Madrid, Campus de Cantoblanco, C/ Francisco Tomás y Valiente, 28049, Madrid, Spain
[c] SustEC-Laboratório Associado para a Sustentabilidade e Tecnologia Em Regiões de Montanha, Instituto Politécnico de Bragança, Campus de Santa Apolónia, 5300-253, Bragança, Portugal
[d] Departamento de Ingeniería Química y Tecnología Farmacéutica, Facultad de Ciencias, Sección de Química, Universidad de La Laguna, Av. Astrofísico Fco. Sanchez S/n, Apdo. 456, 38200 La Laguna, Tenerife, Spain
[e] Department de Química, Facultat de Ciències, Universitat de Girona, C/ Mª Aurèlia Capmany, 69, 17003, Girona, Spain

ARTICLE INFO

Keywords:
Soil humic acids
Volcanic ash soil
PPCPs
PPCP-HA interaction
Adsorption isotherms
Reclaimed water

ABSTRACT

A multidisciplinary approach investigates the interaction between selected PPCPs with diversified physico-chemical propertiesand humic acids (HAs) extracted from Elliot and volcanic soils in reclaimed water (RW). Principal component analysis (PCA) reveals significant differences between the two HAs and how these differences affect PPCP-HA interaction which are characterized by UV spectroscopy. The sorption of PPCPs on either IHSS HA or CAN HA fit a pseudo-second-order kinetic reaction in RW, indicating that the adsorption rate was controlled by the diffusion of the PPCP, followed by adsorption on the HA surface. The sorption of each individual PPCP on both HAs was characterized by applying sorption isotherm models, showing that chemisorption is involved. Moreover, the simultaneous PPCP-HA interactions between the selected PPCPs and both HAs in RW (at different pHs) fitted Freundlich's model ($R^2 > 0.9890$), where, K_F values are 0.0003 and 0.085 for simultaneous adsorption on IHSS HA and CAN HA, respectively. The greater K_F value obtained for CAN HA suggests that the simultaneous PPCP adsorption is more favourable in this HA than in IHSS HA. Meanwhile, coexisting Ca^{2+} (>50 mM) in RW could inhibit the PPCP–HA interaction due to the aggregation of HAs. This study highlights the importance of the HA origin in the interaction with PPCPs in RW, which can affect the fate and transport of these pollutants and the associated environmental risk.

1. Introduction

Across the EU, agriculture alone accounts for approximately 59 % of all water used, a figure which reaches 80 % in southern European countries. The scarcity of water and increasingly frequent droughts make water reclamation an issue of the utmost importance in the Canary Islands (Spain), where the present study takes place. Territories which are highly dependent on groundwater given the lack of other freshwater sources, such as rivers or lakes (Santamarta et al., 2022). The challenges in removing PPCPs from wastewaters even during advanced treatment processes have been shown by recent studies (Mladenov et al., 2022; Marino et al., 2025). Notably, the mobility, distribution and ecological hazards of PPCPs are intimately related to their physico-chemical properties. Beside that even a slow transport of PPCPs through reclaimed water for irrigation and the soil layer can contaminate groundwater (Chakraborty et al., 2023).

Regulation 2020/741/EU/2020 of the European Commission sets minimum physico-chemical and microbiological parameters for the use of reclaimed water in agricultural irrigation (Tajima et al., 2020). However, emerging contaminants are not considered, even though there is concern regarding their potential effects on crops (García-Valverde et al., 2023). Moreover, the presence of these micropollutants affects chlorophyll content, flowering and germination rates in plants.

The organic matter (OM) also present in reclaimed water for crop irrigation may also influence soil health. Dissolved organic matter (DOM, size <0.45 μm) accounts for between 78.1 % and 86.5 % of

☆ This paper has been recommended for acceptance by Dr Jiayin Dai.

* Corresponding author.
E-mail address: empena@ull.edu.es (P.-M. EM).

https://doi.org/10.1016/j.envpol.2025.127163
Received 22 July 2025; Received in revised form 10 September 2025; Accepted 23 September 2025
Available online 26 September 2025

dissolved organic carbon and between 82.6 % and 86.6 % of total organic carbon in the effluent of wastewater treatment plants (WWTPs) (Wang et al., 2014; Fuentes-Rivas et al., 2020). Among the compounds present in DOM, humic substances and their component HAs interact with and adsorb PPCPs in both water and soil, governing reactivity, bioavailability, toxicity, and the transport of these contaminants through a diverse range of geochemical and environmental systems (Ampong et al., 2022; Shanying et al., 2022; Zheng et al., 2022). Therefore, it is important to understand the interaction mechanism between the HA domain and families of PPCPs (Kulikova, 2022).

Humic substances, which are widely distributed in soil and water, whose composition and structure vary depending on their geographical origin, age, climate and abiotic and biotic conditions. The high aromaticity and molecular condensation of humic substances in volcanic ash-derived soils were formerly ascribed to the catalytic effect of amorphous materials in the polycondensation of soluble precursors of the HAs (Hernández et al., 2012; Hernández and Almendros, 2012). A previous study detected substantial amounts of chitin-derived and other carbohydrate-type compounds or alkyl C in the soil OM of Andosols, which depends on the content of amorphous minerals in the soil (González-Pérez et al., 2012; Rivas et al., 2012). These substances could have a noticeable effect on the reactivity and condensation process (Almendros et al., 2018), affecting the adsorption rate of pollutants such as the PPCPs. In the case of HA from volcanic ash soils, this effect could be ambivalent since contaminant retention on the surface could be favoured by carboxyl or hydroxyl (–OH) groups or influenced by metal-ligand relationships or isomorphic or redox substitutions.

The main HA-PPCP interactions are hydrophobic interactions, electrostatic interactions including hydrogen bridges, and π-π interactions between the aromatic groups of HAs and the benzene rings of the micropollutants (Pedrosa et al., 2020). The presence of metal ions such as Ca^{2+} and Mg^{2+} in the aqueous media can result in cationic bridge-type interactions with the functional groups (i.e. –COOH and –OH) of the HAs (Yuan et al., 2018), increasing the aggregation capacity of the HA when the concentration of Ca^{2+} is increased (Kloster et al., 2013). Moreover, the role of pH and DOM on the availability (eg. speciation, complexation, translocation to plants) of PPCPs in water should be also considered (Raya et al., 2017; Aolin et al., 2024). Most of the studies into PPCP−HA interactions based on empirical or qualitative analyses, where intrinsic differences due to the origin and type of HA have not been investigated (Kulikova et al., 2022). Giving as a result a gap in the research about the influence of the origin and concentration of the HAs in their interactions with PPCPs, at the pH and chemical conditions of the aquatic media, that affect deeply the bioavailability of these contaminants in the environment.

The present study aims to characterize the kinetics and the adsorption processes of PPCPs by HAs in RW and to study the effect of the different origins and composition of HA, pHs and RW matrix on their interactions. We selected two HAs, one extracted from Elliott soil (IHSS HA) and another extracted from a Canarian soil (CAN HA). The PPCP-HA interactions were characterized using structural and functional data derived from UV–Vis spectroscopy, high-performance liquid chromatography with a diode array detector (HPLC-DAD), and multivariate statistical analysis. The selection of the target PPCPs was based on their markedly different physico-chemical properties and our knowledge of their frequent presence in RW.

2. Experimental

2.1. Materials and chemicals

The PPCPs chosen included sulfamethoxazole (SMZ, CAS 723-46-6), diclofenac (DCF, CAS 15307-86-5), naproxen (NAP, CAS 22204-53-1), carbamazepine (CBZ, CAS 298-46-4) and triclosan (TCL, CAS 3380-34-5) (see Table S1 for chemical structures and selected physicochemical properties). Ethanol (EtOH), methanol (MeOH), acetonitrile (AcN), sodium hydroxide and sodium azide were all provided by Sigma-Aldrich Chemie GmbH (Steinheim, Germany). Hydrochloric acid, nitric acid and inorganic salts ($MgCl_2{\cdot}6H_2O$, $CaCl_2$, and NaCl) were purchased from Fluka Chemie AG (Buchs, Switzerland). All chemicals were of analytical reagent grade (unless otherwise indicated) and were used as received. The HAs from Elliott Soil IHSS 1S102 were purchased from the International Humic Substances Society (IHSS, USA). The PPCP stock solutions were prepared in ethanol and stored at −18 °C under dark conditions. Working standard solutions were prepared daily using ultrapure water at the desired concentration levels by diluting the analyte mixture solutions.

Ultrapure water was obtained from Purelab Flex ElGA Veolia ultrapure water supplied by VWS (UK). All glassware was rinsed with 10 % nitric acid and ultrapure water several times before use. Iso-disc™ filters, PTFE-4-2, 4 mm × 0.2 μm were obtained from Supelco (Bellefonte, PA, USA).

2.2. UV–Vis spectrophotometry

Spectroscopic analyses were conducted with an UV–Vis spectrophotometer Cary 50 Conc (Varian, Inc., The Netherlands). The performance of the UV–Vis spectroscopic analytical method for PPCPs was established by determining the analytical quality parameters (Table S2 A). UV–Vis spectral indicators for HA, including the E2/E3 ratio of the HA absorbance at 280 and 360 nm, the E4/E6 ratio (HA absorbance at 465 nm was divided by the value measured at 665 nm) and the log ΔK = log A400 − log A600, were calculated.

2.3. Liquid chromatography – diode array detector (HPLC-DAD)

The concentration of the selected PPCPs was quantified by HPLC-DAD with a Varian 920 LC system equipped with a quaternary pump, auto sampler and diode array detector using Galaxie Workstation Chromatography Data System software (Varian Inc., Australia). Chromatographic separations were achieved using a microsorb C18 column (25.0 cm × 4.6 mm × 8 μm) at 303 K provided with a Chromguard pre-column, both from Varian Inc. (California, USA). The mobile phase comprising A: B (80 % acetonitrile: 20 % H_3PO_4 (0.2 %, pH 2.7) was applied at a 1 mL/min flow rate. The signals were acquired with a diode array detector.

The performance of the analytical method was established by determining the analytical quality parameters (Table S2 B). The limit of detection (LOD) and limit of quantification (LOQ) of the analytical procedure were determined using the signal/noise ratio. The matrix effect of RW in determining PPCP concentrations by HPLC-DAD was assessed, and the results showed that the standard deviation of the detection signals was lower than 3 % compared with those obtained in ultrapure water.

The pH was measured using a pH meter (PH 197-S) equipped with a SenTix-81 pH electrode from WTW (Weilheim, Germany) and an Inlab® micro-pH electrode from Mettler Toledo (Barcelona, Spain). Standard buffer solutions of Panreac (Barcelona, Spain) were used for the calibration.

2.4. The characterization of humic acids

The chemical characterization of HA can be screened by different techniques, allowing the structure, composition, size, and morphology to be analysed (IHSS, 2024). The extraction and isolation of HA from soil was done with aqueous NaOH, followed by precipitation of HA at low pH and a series of desalting steps involving cation exchange and dialysis (Hernández and Almendros, 2012; IHSS, 2024).

The particle size distribution and zeta-potential were measured at different pHs using a Malvern Zetasizer Nano ZS, Micromeritics AUTOCHEM 2920, a pH meter equipped with an Inlab® micro-pH electrode from Mettler Toledo (Barcelona, Spain), and an IKA

Labourtechnik RCT B S1 stirrer-hot plate from IKA (Staufen, Germany).

Elemental analysis was conducted using a CHNSO PerkinElmer 2400 elemental analyser to determine the carbon (C), hydrogen (H), nitrogen (N) and sulphur (S) content of the HAs samples.

The textural properties of the HAs were determined from N_2 adsorption–desorption isotherms at 77 K, obtained in a Quantachrome NOVATOUCH XL4 adsorption analyser. The surface area (S_{BET}) was determined by the BET (Brunauer-Emmett-Teller) method. The external surface area (S_{ext}) and the micropore volume (V_{mic}) were obtained by the t-method (thickness was calculated by employing ASTM standard D-6556-01).

Fourier transform infrared (FTIR) spectra were recorded with an Agilent Cary 630 FTIR spectrometer (Agilent, Santa Clara, USA) equipped with a diamond attenuated total reflectance (ATR) accessory. The CPMAS ^{13}C nuclear magnetic resonance (^{13}C NMR) spectra were also acquired in the solid state with a Bruker MSL100 spectrometer (2.3T) at 25.1 MHz. The whole ^{13}C spectra were divided into the following ranges: 0–46 ppm = alkyl C; 46–110 ppm = O-alkyl C; 110–160 ppm = aromatic C (ca.126 = aromatic C–H); 160–220 ppm = C=O-C.

To determine the molecular composition of soil HAs, pyrolysis combined with gas chromatography mass spectrometry (Py-GC/MS) analyses were conducted on a pyrojector (SGE Analytical Science, Melbourne, Australia) connected to a GC/MS system Finnigan Trace GC Ultra with a Trace dual stage quadrupole (DSQ) mass spectrometer (Thermo Finnigan LLC, Austin TX, USA). The identification and relative quantitation of pyrolysis products were carried out by selecting fragments in ion chromatograms for the major compound series, compared with our own laboratory databases of chromatographic compound data of commercial standards and from the automatic search engines of the NIST and Wiley libraries.

2.5. Samples

2.5.1. Reclaimed water (RW)

RW from the tank (Fig. S1) was collected in polyethylene containers and preserved at 4 °C until analysis, which took place within 24 h. Before extraction, samples were filtered through an 0.45 μm filter (Chromafil® XtraPET-45/25 filter, Macherey-Nagel GmbH & Co, UK). Finally, the samples were filtered through 0.20 μm Iso-disc™ filters before HPLC-DAD analysis (Fig. S2). The analyses were performed following the standard methods of the Water Analysis Laboratory of the University of La Laguna. The water quality parameters measured in the RW included pH, electrical conductivity (EC), total suspended solids (TSS), biological oxygen demand after 5 days (BOD_5), chemical oxygen demand (COD), and the anion and cation content: NO_2^-, PO_4^{3-}, K^+, Na^+, HCO_3^-, SO_4^{2-}, Cl^- and F^- (Fig. S3).

2.5.2. Humic acids (HA)

HAs from two different soils were used: a standard HA from Elliott soil (IHSS HA) and an HA from the Canary Islands (CAN HA). The CAN HA sample was obtained from an Andosol of the Canary Islands (Spain, 28°28′ N and 16°29′ W) developed from volcanic ashes, giving andic properties, including a high content of amorphous minerals (Hernández et al., 2012). A brief chemical description of both HAs is included in Table S3.

Stock solutions of 200 mg/L of each HA (soil IHSS and Canarian) were prepared by dissolving the corresponding weight in 36 mM NaOH (Pacheco et al., 2003; Peña-Méndez et al., 2005).

2.6. Interaction mechanism between PPCPs and humic acids by UV–Vis spectrometry and HPLC - DAD

2.6.1. Characterization of the interaction of target PPCPs and HAs by UV–vis spectrometry

HA solutions were spiked with different concentrations of each PPCP to study their interactions by UV–Vis spectrometry. This was done in order to select the best experimental conditions for the identification and assessment of the most significant processes and effects. Individual PPCP solutions were added to an HA solution in 15 mL tubes, resulting in a PPCP concentration of 6.0 mg/L. The concentration of HA varied from to 5–30 mg/L, always giving a total volume of 10 mL and a pH of 8.2 ± 0.3. The solutions were then agitated at 30 rpm in a laboratory rotatory agitator at a temperature of 298 K. Finally, the UV–Vis absorption spectra of the mixture solutions were recorded. A direct comparison of all indicators and parameters between spiked HA with PPCP standard solutions and HA solutions (aqueous samples) was undertaken, allowing the identification and assessment of the most relevant processes and effects.

2.6.2. Sorption experiments of PPCP by HAs in water and RW

Batch sorption experiments were performed in 15 mL tubes using each HA as adsorbent and the target PPCP as the adsorbate in aqueous solutions. HA concentrations varied from 10 to 75 mg/L, whereas a fixed concentration of PPCP of 10 mg/L was chosen to monitor the PPCP signals in the solution. According to Spanish regulation for RW (Real Decreto 1620/2007; Real Decreto 1085/2024), the pH values of this water for irrigation uses should range between 7 and 9; therefore, the experiments were run at pH 7.0 ± 0.3 and pH 9.0 ± 0.3.

The pH of the HA solution was adjusted at the desired pH before adding the PPCP solution using HNO_3 (1M) and NaOH (1M). The kinetics and the characterization of the adsorption processes were performed by analyzing the adsorption data at pH 7.0 in aqueous media. Moreover, the effect of time on the percentage of adsorption of each PPCP was also studied in RW.

Given that Ca^{2+} is present in RW (Fig. S3), the potential influence of Ca^{2+} on the interaction of PPCP–HA in this water was investigated by spiking 10 mg/L HA colloidal solutions with 10 mg/L of the target PPCP and two concentration levels of Ca^{2+}, 0.25 and 0.50 mmol/L, at pH 7.0 ± 0.3. The mixtures were agitated for 1 h, and HPLC-DAD was used to determine the concentrations of PPCPs remaining in the solutions, which were compared with those obtained under the same conditions in RW without adding Ca^{2+}.

Sample aliquots were collected at specified intervals and analysed by HPLC-DAD. In addition, a set of blank experiments was run under the same conditions to determine the matrix influence. All experiments were performed in triplicate and simultaneously with and without HA to assess the effect of the selected PPCP has on the HA structure.

2.6.3. Method validation

The analytical methodologies were validated according to EU quality control procedures SANTE 11312/2021 (Pihlström et al., 2021). The linearity, matrix effect, sensitivity, trueness (in terms of recovery), precision (in terms of method repeatability and reproducibility) and selectivity were evaluated for each matrix studied (ultrapure and RW). Blank samples of both matrices were also analysed to assess the selectivity and specificity of the method. No other peaks caused by co-eluting interferences from the matrices were detected for the target analytes (i.e., PPCP) in a retention time range of ±0.2 min.

2.7. Statistical analyses

The data were prepared and processed using Microsoft Excel software. All statistical analyses were performed using SPSS v.29 for Windows (IBM SPSS Statistics). Significant differences ($p \leq 0.05$) in measurements between HA and PPCP−HA (source: CAN HA and IHSS HA) were analysed using ANOVA (paired with Tukey Honest Significance Difference (HSD) tests). Principal component analysis (PCA) was used to identify patterns in data and relationships between variables (Deulofeu et al., 2019).

3. Results and discussion

3.1. Characterization of humic acids

The H-to-C and O-to-C atomic ratios are commonly used to illustrate diagenetic transformation processes of bio- and geo macromolecules such as HAs. In the case of CAN HA, the atomic ratios are closer to lignin-type plant biomacromolecules, whereas the decrease of the H-to-C and O-to-C ratios in IHSS HA is attributed to a high aromatization and condensation (Table S3).

An intensive band at 2920 cm^{-1} (Fig. 1A) in the FTIR spectra is assigned to C–H aliphatic stretching, the band at 1460 cm^{-1} is related to the symmetric bending of methoxyphenols, whereas the band at 1720 cm^{-1} is ascribed to C=O stretching vibrations of carboxyl groups. A series of overlapping vibrations of carbonyl functions and quinones is assigned to the intensive bands at 1620 cm^{-1}, and the bands close to 1230 cm^{-1} are associated with O-H stretching vibrations of carboxyl groups. It should be noted that the IR spectrum for IHSS HA presents greater intensity in the 1720 cm^{-1} and 1230 cm^{-1} bands, which indicates greater relative abundance of carboxyl groups.

The ^{13}C NMR spectra of both HAs showed the most intense aromatic C signal peaking at 126 ppm (Fig. 1B). The IHSS HA displayed the highest carbonyl C signal (carbonyl region) at 172 ppm, assigned to carboxyl and H-containing groups, and weak alkyl signals at 33, 56 or 73 ppm, suggesting a low aliphatic domain. However, CAN HA had a high alkyl and O-alkyl ^{13}C NMR signal intensity (0–46 and 46–110 ppm, respectively) and an intermediate signal intensity in the 110–160 and 160–220 ppm ranges, associated with aromatic and carbonyl C, respectively, suggesting a comparatively high structural diversity with both aliphatic and aromatic domains. CAN HA shows high optical

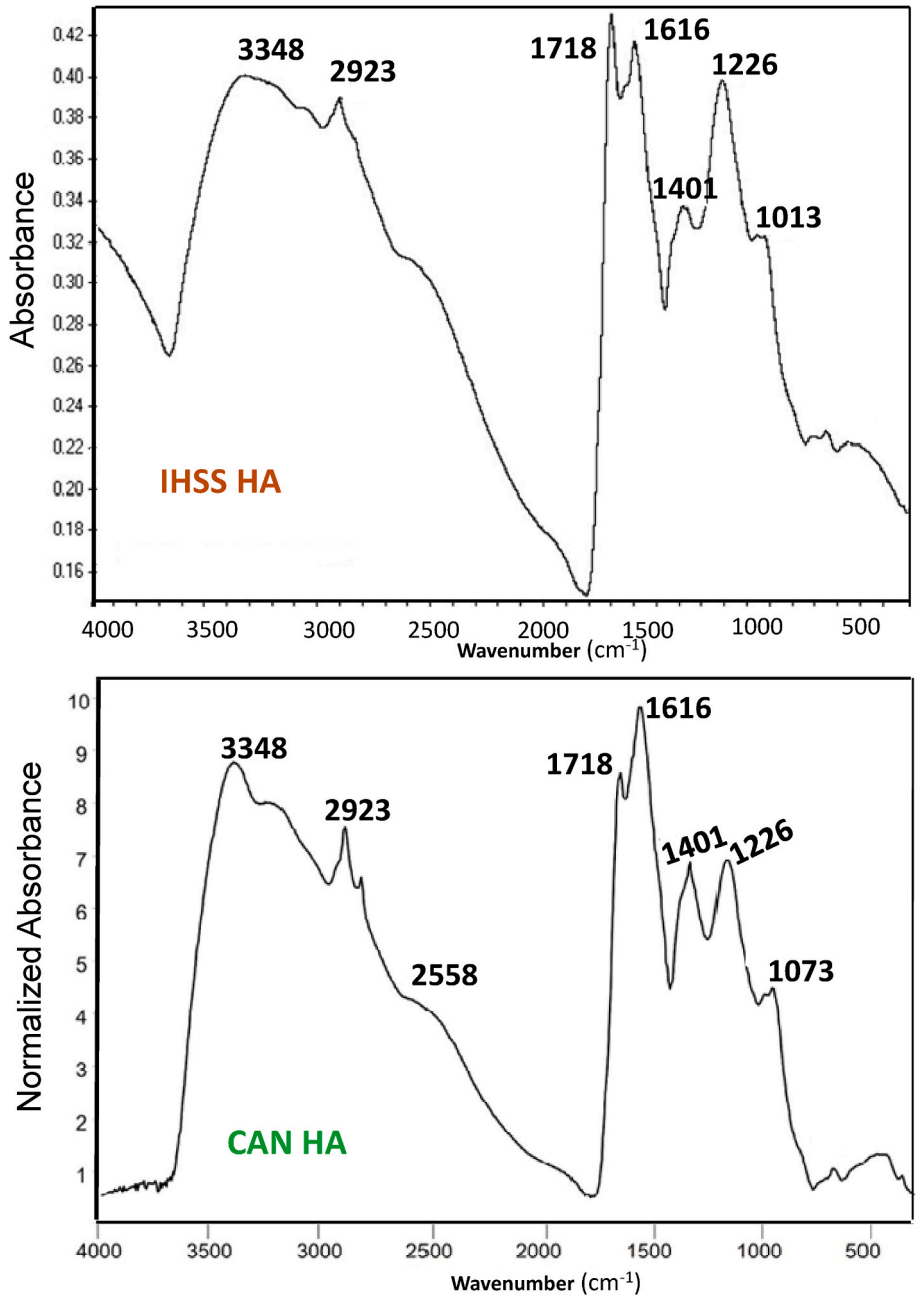

Fig. 1. A IR spectra of Elliot HA and CAN HA.
B ^{13}C NMR spectra of Elliot HA and CAN HA.

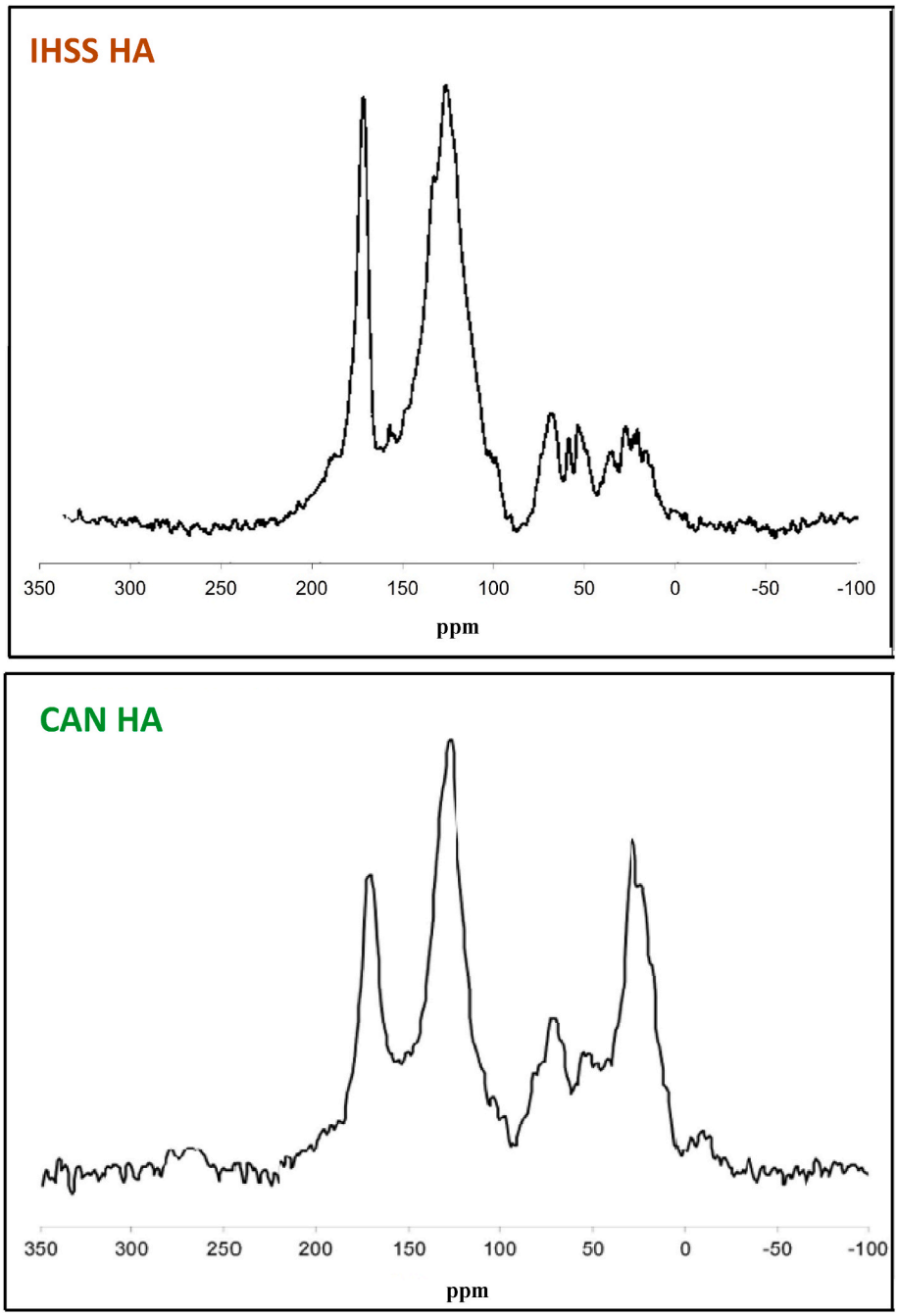

Fig. 1. (*continued*).

density values at 465 nm (E4), which is related to the aromaticity of HA that probably originates in fungal pigments (quinones) that were identified in the second derivative of the visible spectrum using standard samples (Table S3).

The results of pyrolytic analysis of the CAN HA showed a low predominance of lignin pyrolysis products (8 % of the total ion chromatographic area), indicating a high degree of lignin alteration, a substantial number of polysaccharides (46.8 %) and N-containing compounds (11.8 %). Some of these pyrolysis products could derive from amino acids and peptides from microbial sources, whose activity is favoured in Andosols containing amorphous minerals (Hernández et al., 2012). Finally, in CAN HA a series of unspecific aromatic compounds such as phenols, benzenes, and naphthalenes were frequently detected as pyrolysis products, and alkylbenzenes made up 16.4 % of these compounds (Table S3).

With regards to physical characteristics, a noticeably low BET specific surface area (8.33 $m^2\ g^{-1}$) was observed in CAN HA with an external specific surface area (Sext) of 6.34 $m^2\ g^{-1}$, a micropore volume (V_{mic}) of 0.001 $mm^3\ g^{-1}$, and an average pore width (W_{mic}) of 0.0016 nm, which indicates that the absorption/desorption curves of CAN HA mainly respond to chemical processes given the low physical reactivity and porosity of the material.

3.2. *Binding of PPCPs to humic acids in reclaimed water*

3.2.1. ***Reclaimed water – physicochemical characterization***

The physico-chemical quality parameters of RW were measured following irrigation water quality guidelines (Real Decreto 1620/2007) and are presented in Fig. S3. Sodium, potassium and chloride concentrations in the samples ranged from 113 to 159 mg/L (mean ± standard

deviation = 136 ± 23 mg/L), and 30.3 to 19.7 (25.1 ± 5.5 mg/L), and 33.55–98 mg/L (65.8 ± 32 mg/L), respectively. The wide variability of sodium and chloride concentrations is associated with the performance of the electrodialysis self-reversal (EDR) system, which is applied to remove salts from the membrane bioreactor (MBR) permeate. Moreover, the volcanic origin of the groundwater and the sea aerosols explain the high content of dissolved salts in the treated water. These should be removed to ensure that the quality parameters for using this water in agricultural irrigation are met. However, only one part of the MBR permeate is treated by EDR, and the reclaimed water tank is filled with a mixture of the MBR permeate and EDR effluent. Their proportions fluctuated depending on the EDR performance and sampling time throughout the day; resulting in variability in the concentrations of sodium and chloride in the treated water. On the other hand, chemical oxygen demand (COD) oscillation is noticeably low since the reduction in COD is mainly due to the ultrafiltration membrane of the MBR.

3.2.2. *The applicability of UV–Vis spectroscopy to characterize and differentiate PPCP−HA interaction*

The unique structures and functional groups of HAs independently of their origin show potential to interact in different modes with small organic contaminants (Chen et al., 2024). Five PPCPs that have been found to be highly prevalent in RW – sulfamethoxazole (SMX), naproxen (NAP), carbamazepine (CBZ), diclofenac (DCF), and triclosan (TCL) – were selected as models for the study (Chtourou et al., 2018; Villanueva-Rodríguez et al., 2019; Beltrán et al., 2020). The structures and physico-chemical properties of these compounds are presented in Table S1.

The interactions between CAN HA and IHSS HA and the selected PPCP were monitored by examining the changes in the UV–Vis spectrum of each HA when the target PPCP was present in the solution at pH = 8.2 ± 0.3. Fig. S4 shows the speciation diagrams vs. pH of the target PPCPs. At this pH, electrostatic interactions between the HAs and the target PPCP are favoured by the negative surface charge of both HAs (z-potential: −9.93 mV for IHSS HA and −17.3 mV for CAN HA) that can help to establish strong π-anion interactions with the target PPCP in addition to π−π interactions, and weak H-bond interactions may also take place (Zhou et al., 2014; Osman et al., 2024). Moreover, the HA z-average particle diameter was established to be 442.6 nm for IHSS HA and 1407 nm for CAN IHSS.

The UV–Vis HA (IHSS and CAN) spectra were recorded in the wavelengths (λ) range between 200 and 800 nm for HAs, PPCP and the PPCP−HA mixture. The UV–Vis spectra after spiking with PPCP at 6 mg/L to both HA solutions (10 mg/L), pH 8.2 ± 0.3, are shown in Fig. 2. The changes in the UV–Vis spectra assigned to the PPCP−HA interaction were monitored through the selected spectroscopic indicators for HAs (E2/E3, E4/E6, log ΔK) and the variations in the λ maxima shift (Δλ (nm)) in the spectra of PPCP due to the presence of HA (Table S4). The

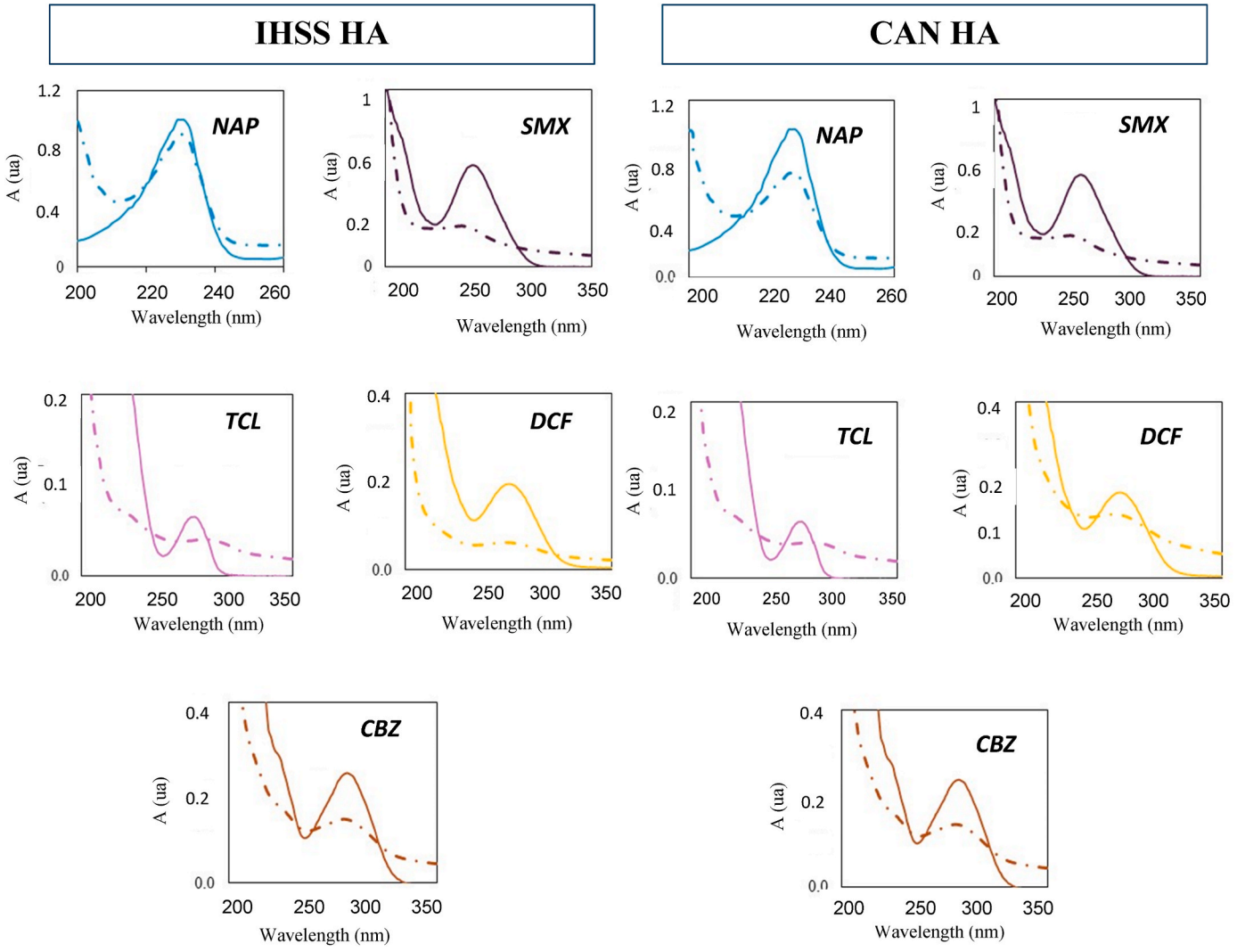

Fig. 2. Normalized UV VIS spectra for the interaction PPCP – HA (IHSS and CAN) in solution (dotted line) and PPCP as reference (continuous line). Conditions: C_{HA} (10 mg/L) PPCP (C_0 6 mg/L) at pH 8.2 ± 0.3.

values of E2/E3 for both HA increased after interaction with the target PPCP. However, the E4/E6 ratio decreased in each HA after interacting with each PPCP, indicating the increased molecular size, degree of condensation and aromaticity of the HAs. The changes in log ΔK depend on the type of HA. In the case of the interaction between PPCP and IHSS HA, there was an increase in the log ΔK, suggesting a decrease in aromaticity (Hernández and Almendros, 2012). However, a decreasing trend was observed for PPCP−CAN HA, except in the case of CBZ. In addition, the UV–Vis spectrum of each PPCP was recorded in the presence of HAs, and a shift, Δλ (nm), corresponding to the maximum of the peaks of the PPCP spectrum is observed except for NAP (Fig. 2).

The spectra of DCF–HA show a shift towards a lower λ, which is Δλ 4 nm for DCF–IHSS HA and 2 nm for DCF–CAN HA. In the case of CBZ–HA, a downward shift of Δλ 3 nm is recorded for both HAs. The Δλ shift of DCF and CBZ spectra also presented band broadening. DCF and CBZ have a similar topological surface area, 49.3 and 46.3 ($Å^2$), but they differ in hydrophobicity as log K_{ow} values are 4.51 and 2.45, respectively. Since the CBZ molecule is neutral (pKa_1 1.97, pKa_2 13.9), the CBZ–HA interaction may be due to π–π staking interactions (Bai et al., 2008). Although DCF is negatively charged at pHs > pKa 4.15, chlorine is present in its structure, suggesting that Cl–π and stacking π-π interactions also occur (Margon et al., 2009; Ye et al., 2022). The spectra of TCL–HA presented a shift to higher wavelengths, $\Delta\lambda_{TCL} = 5–6$ nm, for both IHSS HA and CAN HA. TCL has a pK_a value of 7.9 and a hydrophobic nature (log Kow of 4.76) that is maintained even in the ionic form. The interaction between TCL and HA could be explained through increasing π interaction in the benzene rings due to the formation of Cl–π and stacking π-π interactions even when TCL is present in its anionic form. Moreover, the electrostatic repulsion forces will be established with negatively charged HA (Liang et al., 2020). UV–Vis spectra of SMX showed band broadening and the greatest shift, $\Delta\lambda_{SMX} = 7$ nm, towards lower λ values after interacting with both HAs. Chen et al. (2017) proposed that sulphonamide antibiotics such as SMX (pKa_2 5.81) tended to interact electrostatically with HAs despite its low log K_{ow} of 0.89 and greater topological surface area 107 $Å^2$ (Table S1). The main adsorption mechanism of SMX on HA was also found to be the hydrogen bonding of aromatic carboxyl or hydroxyl groups on HA with amide in SMX (Liu et al., 2023).

A marked band broadening at lower wavelengths (200–220 nm) and a decrease in the maximum NAP peak were observed in the UV–Vis spectra of NAP in the presence of both HAs. However, there was no observable Δλ shift in the spectra. Considering the hydrophobicity of NAP (log K_{ow} 3.18) and its pKa (4.15), a decrease in the interaction/sorption NAP–HA can be expected when the pH increases (Wojcieszyńska and Guzik, 2020). The results above imply that HA can temporarily fix NAP through weak H-bond interactions.

The interaction between small organic contaminants such as PPCP and HAs can be driven by different processes that may act individually or synergistically. Considering that the UV–Vis spectra represent the fingerprint spectra of a multicomponent system of each PPCP with the two types of HAs, a qualitative assessment of UV–Vis spectra (HA and PPCP + HA) was performed by principal component analysis (PCA), which allows insights and patterns to be revealed. The PCA scores plot (Fig. 3) depicts the three first principal components (PC), explaining 98 % of the variance. The position of the samples in Fig. 3 illustrates the differentiation of PPCP−HA interaction and HA, differentiating the more aromatic nature of IHSS HA from the aliphatic or o-alkyl nature of CAN HA. In contrast, the second PC (PC2) refers to the types of interactions between PPCP and HAs, forming a gradient of variability from DCF, which is hydrophobic (log K_{ow} 4.51), to CBZ, which is of intermediate hydrophobicity (log K_{ow} 2.45) and SMX, which is hydrophilic (log K_{ow} 0.89). One notable exception to these trends where no differentiation is associated with the type of HA is for NAP.

As illustrated by our study, the information obtained by UV–Vis spectroscopy from the different PPCP−HA interactions (HA: CAN and IHSS) is highly complex, but the interaction patterns were differentiable by PCA. However, the interaction mechanism involving PPCP analytes and the transformation of HA substrates after their interaction remains unclear and deserves further study.

3.2.3. PPCP and HA interaction in reclaimed water

The enormous complexity of the organic molecular structure of HA, together with the environmental conditions, regulates the interaction mechanisms with PPCPs. When PPCPs are adsorbed by the HAs, the temporarily transport in RW. Therefore, considering the pH of the RW matrix (7.0 ± 0.3), the PPCP species that are expected to be permanently charged and ionizable are NAP, SMX, DCF; CBZ is neutral, and TCL partially charged (see Table S1 for pKas and Fig. S4). The HA surface becomes predominately negatively charged when the pH values rise as –COOH and –OH moieties present in HA molecules dissociate, expanding the configuration of HA molecules (Tian et al., 2021) and affecting the HA sorption capacities towards PPCP in the RW matrix.

In accordance with the present legislation, the pH values of RW should range between 7 and 9; thus, the experiments were run at pH 7.0 ± 0.3 and pH 9.0 ± 0.3 in ultrapure water (Fig. 4). In the case of IHSS HA, less than 90 % of the initial concentration of each PPCP, except TCL,

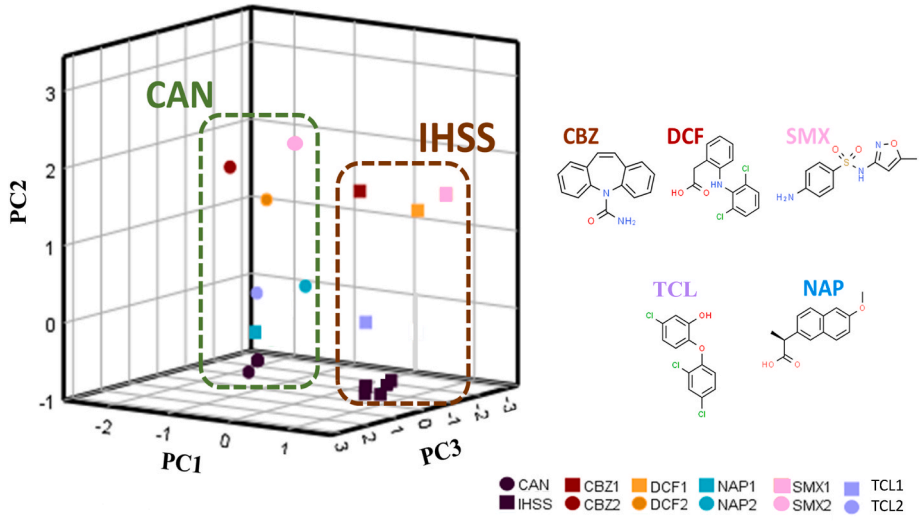

Fig. 3. Scores plot for PCA of UV–Vis spectra of HA (CAN and IHSS) and the interaction PPCP-HA.

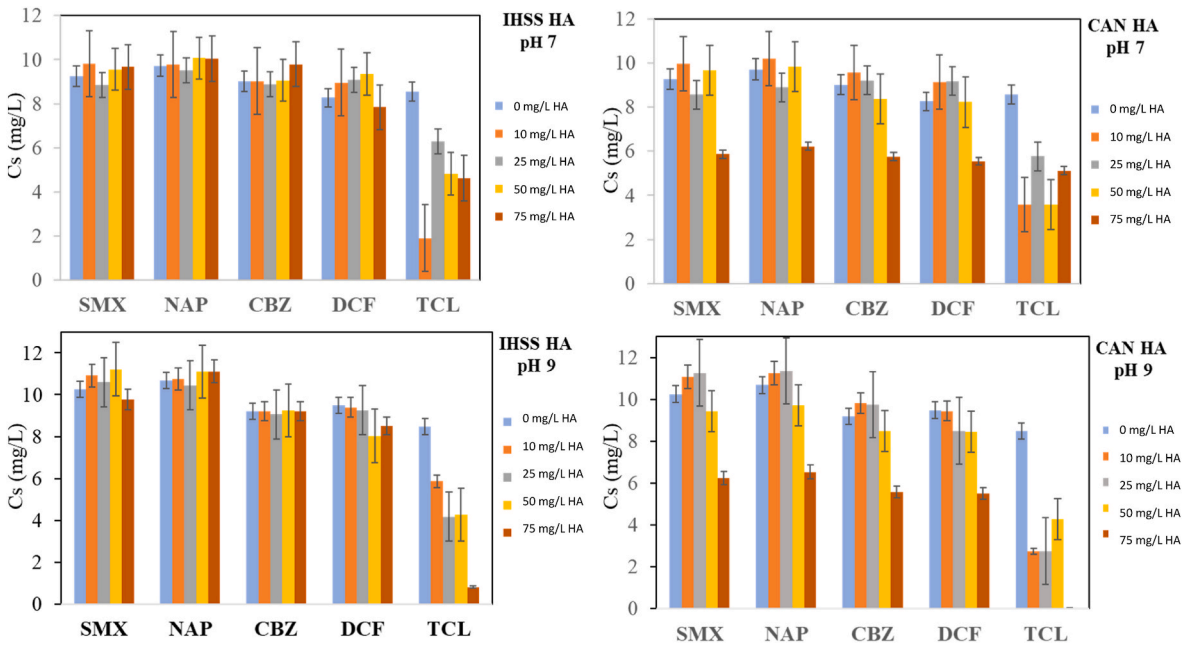

Fig. 4. PPCP concentrations remaining in the water solution after interaction with HA (IHSS and CAN) at different pHs. (PPCP C_0: 10 mg/L, t 1h).

remained in solution at both pH conditions after 1 h of agitation. TCL was the most adsorbed PPCP by IHSS HA with a maximum adsorption percentage of 90 % for a concentration of 75 mg/L at pH 9.0 whereas at pH 7.0 and with the same IHSS HA concentration, the adsorption percentage was ~55 %. As can be seen in Fig. 4, higher adsorption percentages ranging from ~30 to 60 % were obtained for all PPCPs on CAN HA when the HA concentration was 75 mg/L at both pHs, with TCL is the most adsorbed compound in accordance with its higher hydrophobicity. These results suggested that in these conditions, the interaction between HA and PPCP species may take place through π-π interactions, although charged-assisted hydrogen bonds could be involved (Sigmund et al., 2022; Xiao et al., 2022; Liu et al., 2023).

In the case of RW, equilibrium was reached after 48 h. Kinetic data corresponding to the two components' systems showed that, the adsorption rate increased rapidly and then slightly decreased until reaching equilibrium (Fig. S5). The results in Table 1 indicate that the kinetic data for the sorption of PPCP on IHSS HA fit a pseudo-second-order kinetic reaction for NAP, SMX, CBZ and TCL with $R^2 > 0.94$ and $R^2 \sim 0.70$ for DCF; and for NAP, SMX, DCF, CBZ and TCL, all of these with $R^2 > 0.92$, when adsorbed on CAN HA. These results indicate that the adsorption rate was controlled by the diffusion of the PPCP, followed by adsorption on the HA surface. However, in all the fitting of the data ($R^2 > 0.80$) to the intraparticle diffusion model confirms this mechanism.

Table 1
Pseudo second order kinetic constants for the adsorption of PPCPs onto HA (IHSS HA and CAN HA).

HA	PPCP	Pseudo 2nd order			Intraparticle diffusion		
		q_e (mg/g)	K (g/mg•h)	R^2	K_{id} (mg/g•min)	C	R^2
IHSS HA	***SMX***	4.17	0.05	0.9521	0.745	0.0632	0.9463
	NAP	12.7	0.012	0.9949	1.33	9.8	0.8816
	CBZ	3.56	16.8	0.9457	1.56	2.9	0.8657
	DCF	16.1	3.73	0.7235	0.886	6.60	0.8179
	TCL	84.5	0.71	0.9998	8.00	33.4	0.8874
CAN HA	***SMX***	2.53	23.7	0.9854	3.94	0.671	0.9898
	NAP	31.8	0.020	0.9580	5.60	4.30	0.8638
	CBZ	96.0	0.62	0.9253	6.00	20.0	0.8323
	DCF	65.2	0.92	0.9904	4.74	13.3	0.8135
	TCL	88.2	0.68	0.9995	8.53	32.2	0.9244

q_e adsorption capacity at equilibrium k_2 rate constants of the pseudo second order kinetic model, t time, K_{id} rate constant of intraparticle diffusion, and C refers to the boundary layer thickness.

Equilibrium experimental data (Fig. 4), obtained from adsorption experiments of each individual PPCP and HA as adsorbent, were analysed using Henry, Freundlich and Temkin adsorption isotherm models (Table 2). Henry's model satisfactorily described the adsorption of SMX ($R^2 = 0.9854$), CBZ ($R^2 = 0.9646$) and DCF ($R^2 = 0.9926$) on IHSS HA indicating a monolayer adsorption of these PPCPs, while for TCL adsorption the data seem to fit the Temkin model ($R^2 = 0.8250$), which is associated to multilayer adsorption processes. With regards to the adsorption of PPCPs to CAN HA, SMX and CBZ fit Freundlich's model ($R^2 \geq 0.9789$), which considers different adsorption sites on the adsorbent surface characterized by different adsorption energies, and NAP fits Henry's model ($R^2 \geq 0.942$). TCL is the exception in the case of both HAs, with no clear fitting of the experimental data to the adsorption models tested. The different interaction observed indicates the importance of the position of the active sites on the HA structure. Moreover, even though the adsorption may be driven by steric hindrance of PPCP molecules, other interactions should not be discarded, as can be seen in Fig. 3 and is explained above (cf. PCA in UV–Vis data).

he simultaneous adsorption of the selected PPCPs by HAs was estimated by assuming that the total amount of PPCPs adsorbed by each HA can be calculated as q_t (mg/g) = $q_i + \ldots + q_n$, and the total concentration at the equilibrium as C_t (mg/L) = $C_i + \ldots + C_n$ (n = number of analytes) (Conde-Cid et al., 2020). Then, q_t (mg/g) = $q_{SMX} + q_{NAP} + q_{CBZ} + q_{DCF} + q_{TCL}$ and C_t (mg/L) = $C_{SMX} + C_{NAP} + C_{CBZ} + C_{DCF} + C_{TCL}$. Following this approach, the data from experiments were used to study adsorption isotherms (Table 2).

It was found that Freundlich's model presents the best fit to experimental data ($R^2 > 0.9890$). In this empirical model, the Freundlich's equilibrium constant K_F represents a measure of adsorption strength, while n is related to the energetic heterogeneity of the adsorbent surface. K_F values are 0.0003 and 0.085 for simultaneous adsorption of all PPCPs on IHSS HA and CAN HA, respectively. The greater K_F value obtained for CAN HA suggests that the simultaneous PPCP adsorption is more favourable in this HA than in IHSS HA. The n values of 0.35 and 0.78 for IHSS HA and CAN HA indicate that the latter has a more heterogenous energy relative distribution of the adsorbate sites. Moreover, a

Table 2
Fitting of experimental data (from binary and six components' systems) to the Henry, Freundlich and Temkin adsorption models.

HA	PPCP	Henry		Freundlich			Temkin		
		$q_e = K_p C_e$		$q_e = K_F C_e^{1/n}$			$q_e = \frac{RT}{b_T} \ln (A + C_e)$		
		K_p	R^2	K_F (mg/g)	1/n	R^2	b_T	A	R^2
IHSS HA	SMX	0.694	0.9854	$3.0 \cdot 10^{-8}$	12	0.9789	587	0.501	0.9092
	NAP	0.0781	0.6115	–	–	–	–	–	–
	CBZ	0.125	0.9646	–	–	–	9591	5.14	0.9870
	DCF	0.0952	0.9926	–	–	–	5393	0.646	0.7786
	TLC	0.538	0.7126	–	–	–	3181	0.699	0.8250
	SMX + NAP + CBZ + DCF + TCL	0.265	0.8537	0.0003	2.9	0.9895			
CAN HA	SMX	0.258	0.9116	0.471	1.2	0.9789	165	0.124	0.9590
	NAP	0.135	0.9642	–	–	–	7232	3.2	0.6417
	CBZ	–	–	0.526	0.3	0.9816	–	–	–
	DCF	–	–	0.025	2.5	0.7970	–	–	–
	TLC	–	–	0.192	0.7	0.7902	–	–	–
	SMX + NAP + CBZ + DCF + TCL	0.230	0.9846	0.085	1.3	0.9899			

q_e (mg/g) is the equilibrium adsorbed amount of PPCP on HA, C_e (mg/L) PPCP concentration at equilibrium, K_F (mg/g), n is the Freundlich exponential. coeficient, b_T and A_T are the Temkin binding constants, R universal gas constant, T(°K). temperature and R^2 determination coefficient.

favourable adsorption of $0<n<1$, which is achieved for both HAs, indicates that chemisorption is involved. The model assumes and highlights the importance of multiple active adsorption sites on a heterogeneous HA adsorbent surface.

The results suggest that the HA at vary concentrations can give rise to HA-PPCP interactions, which can affect their environmental transport and, thus, PPCPs speciation and concentration in soil pore water. Water and soil pH affect the contaminants bioavailability and up taking by plants. Alkaline pH conditions produce an increasing microbial grows, which favoured the contaminants degradations (Raya et al., 2017).

3.2.4. *The effect of divalent cations Ca^{2+} and Mg^{2+} on the interaction HA and PPCP in reclaimed water for irrigation*

Ca^{2+} and Mg^{2+} are present in RW, and it has been reported that the presence of Ca^{2+} affects HA aggregation, which can affect the soil structure (Hakim et al., 2019), modifying the charge distribution in the HA surface (Sigmund et al., 2022). These changes will influence the adsorption of PPCPs by HAs. Hence, the potential influence of Ca^{2+} on the interaction of PPCP−HA in RW has been investigated by spiking 10 mg/L HA colloidal solutions with 10 mg/L of the target PPCP and two concentrations of Ca^{2+}, pH 7.0 ± 0.3.

One hour after adding Ca^{2+} (at two concentrations: 0.25 and 0.5 mmol/L) at both IHSS HA and CAN HA solutions (pH 7.0 ± 0.3), the colour became noticeably lighter (Fig. 5A and B) due to the binding of the divalent cation with the –COO^- functional groups of HAs, inducing HA aggregation, as has been described for Leonardite HA under similar conditions (Hakim et al., 2019).

The remaining concentrations of PPCP after 48h, when equilibrium was achieved in the presence of Ca^{2+}, are presented in Fig. 5 (5A and 5B). SMX, NAP, DCF and CBZ concentrations were compared with those obtained in the same conditions without spiking RW samples with Ca^{2+}, and no significant variability ($p < 0.05$) was found for the concentrations of the pharmaceutical compounds, except that there was a significant decrease in the concentrations of TCL. According to the US Environmental Protection Agency (US EPA, 2017; 2024), TCL is stable to hydrolysis at pH 7. However, biodegradation, photolysis, and photochemical reactions are responsible for its decline in natural waterways. Chen et al. (2016) investigated the influence of a commercial HA on the photolysis of TCL species in solution, finding that photolysis was the main process for inhibiting triclosan when HAs were present. This tendency was not observed when TCL was in its anionic form in solution. In addition, the HCO_3^- may contribute to the photodegradation of TCL in

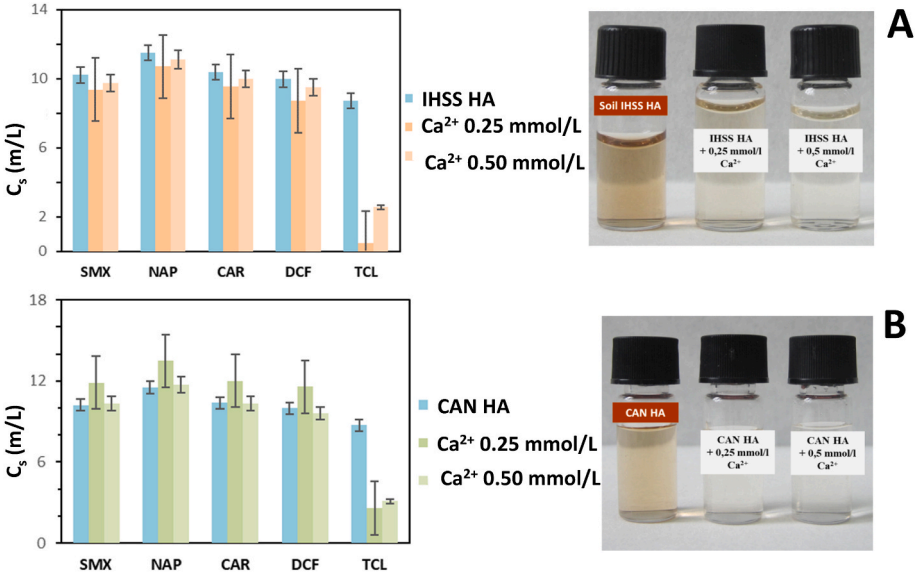

Fig. 5. PPCP concentrations remaining solution of PPCP after interaction with 10 mg/L of IHSS HA (**A**) and CAN (**B**) HA, RW spiked with divalent [Ca^{2+}] at concentrations 0.25 and 0.5 mmol/L (PPCP C_0: 10 mg/L, pH 7.0 ± 0.3, t 1h).

water (Chen et al., 2018). The HCO_3^- concentration in the RW samples used in this study varies between 190.30 and 339.26 mg/L (Fig. S3) and may play a role in TCL degradation. However, the experimental findings described in this manuscript did not give insights that could explain these findings. Further analysis is needed to understand the biodegradation of TCL in scenarios such as HA and RW.

4. Conclusions

The different physical-chemical characteristics of the two HAs permitted the differentiation between PPCP−HA interactions. The characterization of CAN HA shows that it contains more aliphatic domain aromatic compounds, given its volcanic origin, than IHSS HA. PCA also reveals these differences between the two HAs, and shows, in the case of PPCP-HA interactions, a gradient of variability from hydrophobic DCF to hydrophilic SMX.

The adsorption percentages for all PPCPs on CAN HA ranged from ~30 to 60 % when the HA concentration was 75 mg/L at pHs 7 and 9, whereas with IHSS HA lower sorption percentages were obtained in the same conditions. At pH 9, the –OH and –COOH groups of the HA surfaces dissociate, decreasing the effectiveness of the PPCPs−HA interaction. In addition to the changes on the surface of the HA (weak interactions with –OH and –COOH groups), structural π-π type changes occur in the presence of the small organic PPCP molecules in water.

TCL was the compound that was most adsorbed by the two HAs due to its higher hydrophobicity. The PPCP-HA interaction may take place through $\pi - \pi$ interactions, although charged-assisted hydrogen bonds could be involved.

The simultaneous adsorption of the selected PPCPs by HAs was estimated and the resulting data was found to fit the Freundlich's model with K_F values of 0.0003 and 0.085 for IHSS HA and CAN HA, respectively. The greater K_F value obtained for CAN HA indicates that simultaneous PPCP adsorption is more favourable on this HA.

This is a laboratory study that uses RW obtained from a wastewater treatment plant as the aqueous media. The RW samples were spiked with the selected PPCPs at concentrations that enabled investigation of the adsorption process by ensuring their detection in the remaining solution at equilibrium.

Besides the origin of HA, the composition of RW can also affect PPCP-HA interaction. The high concentration of bicarbonates of volcanic origin in RW allows the buffered medium to be maintained at pH 7.00 ± 0.17, increasing the efficiency of the PPCP adsorption on HAs. However, the presence of Ca^{2+} at concentrations >0.05 mM in the water matrix (RW) resulted in a lesser sorption efficiency, clearly as a consequence of Ca^{2+} occupying the exchange positions of the HAs, so reducing PPCP−HA interactions and hence favouring the greater presence of these micropollutants in water.

CRediT authorship contribution statement

J.E. Conde-González: Validation, Supervision, Resources, Project administration, Methodology, Funding acquisition, Conceptualization. **Hernández Z:** Methodology, Conceptualization. **Aguiar V:** Writing – review & editing, Visualization, Validation, Formal analysis. **Vera L:** Resources, Funding acquisition, Conceptualization. **Marrero MC:** Resources, Methodology, Formal analysis, Conceptualization. **Salvadó V:** Writing – review & editing, Validation, Resources, Methodology, Funding acquisition, Conceptualization. **Peña-Méndez EM:** Writing – review & editing, Validation, Methodology, Investigation, Formal analysis, Conceptualization.

Data statement

The datasets generated during and/or analysed during the current study are available from the corresponding author on reasonable request.

Declaration of competing interest

The authors declare that they have no known competing financial interests or personal relationships that could have appeared to influence the work reported in this paper.

Acknowledgements

LV and MCM thank the research project between BALTEN and ULL research teams for partially funding this work. "Tratamiento y Reutilización de Aguas (TyRA)" and "Laboratorio de Agua y Medio Ambiente", del Instituto Universitario de Enfermedades Tropicales y Salud Pública de Canarias (IUETSPC). In addition, the information about the Northeast WWTP supplied by the Consejo Insular de Aguas de Tenerife and SACyR is highly appreciated. V. S. is grateful for the support of the "Un sistema terciario ecoeficiente para la reutilización de agua en riego agrícola (BIODAPH)" research Project (TED2021-132721B-I00/MCIN/AEI/10.13039/501100011033/y Unión Europea "NextGenerationEU"/PRTR).

Appendix A. Supplementary data

Supplementary data to this article can be found online at https://doi.org/10.1016/j.envpol.2025.127163.

Data availability

Data will be made available on request.

References

Almendros, G., Hernández, Z., Sanz, J., Rodríguez-Sánchez, S., Jiménez-González, M.A., González-Pérez, J.A., 2018. Graphical statistical approach to soil organic matter resilience using analytical pyrolysis data. J. Chromatogr. A 1533, 164. https://doi.org/10.1016/j.chroma.2017.12.015.

Ampong, K., Thilakaranthna, M.S., Gorim, L.Y., 2022. Understanding the role of humic acids on crop performance and soil health. Front. Agron. 4, 848621. https://doi.org/10.3389/fagro.2022.848621.

Aolin, H., Qin, L., Zhu, S., Hu, X., Yin, D., 2024. Combined effects of pH and dissolved organic matter on the availability of pharmaceuticals and personal care products in aqueous environment. Sci. Total Environ. 929, 172637. https://doi.org/10.1016/j.scitotenv.2024.172637.

Bai, Y., Wu, F., Liu, C., Guo, J., Fu, P., Li, W., Xing, B., 2008. Interaction between carbamazepine and humic substances: a fluorescence spectroscopy study. Environ. Toxicol. Chem. 27 (1), 95. https://doi.org/10.1897/07-013.

Beltrán, E.M., Pablos, M.V., Fernández Torija, C., Porcel, M.Á., González-Doncel, M., 2020. Uptake of atenolol, carbamazepine and triclosan by crops irrigated with reclaimed water in a mediterranean scenario. Ecotoxicol. Environ. Saf. 191, 110171. https://doi.org/10.1016/j.ecoenv.2020.110171.

Chakraborty, A., Adhikary, A., Bhattacharya, S., Dutta, S., Chatterjee, S., Banerjee, D., Ganguly, A., Rajak, P., 2023. Pharmaceuticals and personal care products as emerging environmental contaminants: prevalence, toxicity, and remedial approaches. CS Chem. Health Saf 30, 362. https://doi.org/10.1021/acs.chas.3c00071.

Chen, K.L., Liu, L.C., Chen, W.R., 2017. Adsorption of sulfamethoxazole and sulfapyridine antibiotics in high organic content soils. Environ. Pollut. 231, 1163. https://doi.org/10.1016/j.envpol.2017.08.011.

Chen, L., Wang, Z., Qian, C., He, Y., 2018. Effects of inorganic anions on the photolysis of triclosan under UV irradiation. Water Sci. Technol. 78, 1476. https://doi.org/10.2166/wst.2018.421.

Chen, J., Zhang, B., Wang, C., Wang, P., Cui, G., Gao, H., Feng, B., Zhang, J., 2024. Insight into the enhancement effect of humic acid on microbial degradation of triclosan in anaerobic sediments. J. Hazard. Mater. 461, 132549. https://doi.org/10.1016/j.jhazmat.2023.132549.

Chtourou, M., 2018. Pharmaceutical and personal Care Products removal by advanced treatment technologies. Thesis. Universitat de Girona. http://hdl.handle.net/10803/664966.

Conde-Cid, M., Ferreira-Coelho, G., Fernández-Calviño, D., Núñez-Delgado, A., Fernández-Sanjurjo, M.J., Arias-Estévez, M., Álvarez-Rodríguez, E., 2020. Single and simultaneous adsorption of three sulfonamides in agricultural soils: effects of pH and organic matter content. Sci. Total Environ. 744, 140872. https://doi.org/10.1016/j.scitotenv.2020.140872.

Deulofeu, M., Kolářová, L., Salvadó, V., María Peña-Méndez, E., Almáši, M., Štork, M., Pour, L., Boadas-Vaello, P., Ševčíková, S., Havel, J., Vaňhara, P., 2019. Rapid discrimination of multiple myeloma patients by artificial neural networks coupled with mass spectrometry of peripheral blood plasma. Sci. Rep. 9, 7975. https://doi.org/10.1038/s41598-019-44215-1.

Fuentes-Rivas, R.M., Martínez-Alva, G., Ramos-Leal, J.A., de León, G.S.C., Moran-Ramírez, J., 2020. Assessment of contamination by anthropogenic dissolved organic matter in the aquifer that underlies the agricultural area. Environ. Sci. Pollut. Res. 27, 45859. https://doi.org/10.1007/s11356-020-10512-w.

García-Valverde, M., Aragonés, A.M., Salinas Andújar, J.A., Gil García, M.D., Martínez-Bueno, M.J., Fernández-Alba, A.R., 2023. Long-term effects on the agroecosystem of using reclaimed water on commercial crops. Sci. Total Environ. 859, 160462. https://doi.org/10.1016/j.scitotenv.2022.160462.

González-Pérez, M., Buurman, P., Vidal-Torrado, P., Martin-Neto, L., 2012. Pyrolysis-Gas Chromatography/mass spectrometry characterization of humic acids in coastal spodosols from Southeastern Brazil. SSSA (Soil Sci. Soc. Am.) J. 76 (3), 961. https://doi.org/10.2136/sssaj2011.0178.

Hakim, A., Suzuki, T., Kobayashi, M., 2019. Strength of humic acid aggregates: effects of divalent cations and solution pH. ACS Omega 4, 8559. https://doi.org/10.1021/acsomega.9b00124.

Hernández, Z., Almendros, G., 2012. Biogeochemical factors related with organic matter degradation and C storage in agricultural volcanic ash soils. Soil Biol. Biochem. 44, 130. https://doi.org/10.1016/j.soilbio.2011.08.009.

Hernández, Z., Almendros, G., Carral, P., Álvarez, A., Knicker, H., Pérez-Trujillo, J.P., 2012. Influence of non-crystalline minerals in the total amount, resilience and molecular composition of the organic matter in volcanic ash soils (Tenerife island, Spain). Eur. J. Soil Sci. 63, 603. https://doi.org/10.1111/j.1365-2389.2012.01497.x.

IHSS, 2024. Standard humic acids and fulvic acids. https://humic-substances.org/.ConsultedSeptember2023.

Kloster, N., Brigante, M., Zanini, G., Avena, M., 2013. Aggregation kinetics of humic acids in the presence of calcium ions. Colloids Surf. A Physicochem. Eng. Asp. 427, 76. https://doi.org/10.1016/j.colsurfa.2013.03.030.

Kulikova, N.A., Solovyova, A.A., Perminova, I.V., 2022. Interaction of antibiotics and humic substances: environmental consequences and remediation prospects. Molecules 27, 7754. https://doi.org/10.3390/molecules27227754.

Liang, S., Xian, Z., Yang, H., Wang, Z., Wang, C., Shi, X., Tian, H., 2020. Rapid destruction of triclosan by Iron(III)-Tetraamidomacrocyclic ligand/hydrogen peroxide system. Chemosphere 261. https://doi.org/10.1016/j.chemosphere.2020.127704.

Liu, F., Li, N., Du, C., Wang, Y., He, K., Zheng, H., Xue, Z., Chen, Q., Li, X., 2023. Various hydrogen bonds make different fates of pharmaceutical contaminants on oxygen-rich nanomaterials. Environ. Pollut. 316, 120572. https://doi.org/10.1016/j.envpol.2022.120572.

Margon, A., Pastrello, A., Mosetti, D., Cantone, P., Leita, L., 2009. Interaction between diclofenac and soil humic acids. Soil Sediment Contam. 18, 489. https://doi.org/10.1080/15320380902962353.

Marino, L., Gagliano, E., Santoro, D., Roccaro, P., 2025. Fluorescence sensor enabled control of contaminants of emerging concern in reclaimed wastewater using ozone-based treatment processes. Water Res. 268 (Part A), 122616. https://doi.org/10.1016/j.watres.2024.122616.

Mladenov, N., Dodder, N.G., Steinberg, L., Richardot, W., Johnson, J., Martincigh, B.S., Buckley, C., Lawrence, T., Hoh, E., 2022. Persistence and removal of trace organic compounds in centralized and decentralized wastewater treatment systems. Chemosphere 286 (1), 131621. https://doi.org/10.1016/j.chemosphere.2021.131621.

Osman, A.I., Ayati, A., Farghali, M., Krivoshapkin, P., Tanhaei, B., Karimi-Maleh, H., Krivoshapkina, E., Taheri, P., Tracey, C., Al-Fatesh, A., Ihara, I., Rooney, D.W., Sillanpaä, M., 2024. Advanced adsorbents for ibuprofen removal from aquatic environments: a review. Environ. Chem. Lett. 22, 373. https://doi.org/10.1007/s10311-023-01647-6.

Pacheco, M.L., Peña-Méndez, E.M., Havel, J., 2003. Supramolecular interactions of humic acids with organic and inorganic xenobiotics studied by capillary electrophoresis. Chemosphere 51, 95. https://doi.org/10.1016/S0045-6535(02)00846-9.

Peña-Méndez, E.M., Gajdošová, D., Novotná, K., Prošek, P., Havel, J., 2005. Mass spectrometry of humic substances of different origin including those from Antarctica: a comparative study. Talanta 67, 880. https://doi.org/10.1016/j.talanta.2005.03.032.

Pihlström, T., Fernández-Alba, A.R., Ferrer Amate, C., Erecius Poulsen, M., Lippold, R., Carrasco Cabrera, L., Pelosi, P., Valverde, A., Unterluggauer, H., Mol, H., Jezussek, M., Malato, O., Štěpán, R., Lambert, M., 2021. SANTE 11312/2021 v2.

Real Decreto 1085/2024, De 22 De Octubre, Por El Que Se Aprueba El Reglamento De Reutilización Del Agua Y Se Modifican Diversos Reales Decretos Que Regulan La Gestión Del Agua. https://www.boe.es/eli/es/rd/2024/10/22/1085/con.

Real Decreto 1620/2007, De 7 De Diciembre Por El Que Se Establece El Régimen Jurídico De La Reutilización De Las Aguas Depuradas. https://www.boe.es/eli/es/rd/2007/12/07/1620.

Regulation 2020/741/EU, 2020. Regulation (EU) 2020/741 of the European Parliament and of the Council, of may 25, 2020, regarding the minimum requirements for the reuse of water. Off. J. Eur. Union 2–32.

Rivas, Y., Matus, F., Rumpel, C., Knicker, H., Garrido, E., 2012. Black carbon contribution in volcanic soils affected by wildfire or stubble burning. Org. Geochem. 47, 41. https://doi.org/10.1016/j.orggeochem.2012.03.007.

Shanying, H., Yufei, W., Chunping, Y., Zhenli, H., 2022. Interactions of microplastics and soil pollutants in soil-plant systems. Environ. Pollut. 315, 120357. https://doi.org/10.1016/j.envpol.2022.120357.

Sigmund, G., Arp, H.P.H., Aumeier, B.M., Bucheli, T.D., Chefetz, B., Chen, W., Droge, S.T. J., Endo, S., Escher, B.I., Hale, S.E., Hofmann, T., Pignatello, J., Reemtsma, T., Schmidt, T.C., Schönsee, C.D., Scheringer, M., 2022. Sorption and mobility of charged organic compounds: how to confront and overcome limitations in their assessment. Environ. Sci. Technol. 56, 4702. https://doi.org/10.1021/acs.est.2c00570.

Tajima, M., Yoshizawa, A., Sakurai, M., Minamiyama, 2020. Establishment of guidelines for the reuse of treated wastewater. The european parliament and the council, regulation (EU) 2020/741, minimum requirements for water reuse. Off. J. Eur. Union 177/33 (2005), 32.

Tian, R., Liu, X., Gao, X., Li, R., Li, H., 2021. Observation of specific ion effects in humus aggregation process. Pedosphere 31, 736. https://doi.org/10.1016/S1002-0160(21)60033-4.

US EPA, 2017. Persistent Organic Pollutants: a Global Issue. A Global Response & International Cooperation. http://chm.pops.int/theconvention/overview/textoheconvention/tabid/2232/default.aspx.

US EPA, 2024. Water Resources of Europe. https://water.europa.eu/freshwater/europe-freshwater/freshwater-themes/water-resources-europe. (Accessed 15 April 2024).

Villanueva-Rodríguez, M., Bello-Mendoza, R., Hernández-Ramírez, A., Ruiz-Ruiz, E.J., 2019. Degradation of anti-inflammatory drugs in municipal wastewater by heterogeneous photocatalysis and electro-Fenton process. Environ. Technol. 40, 2436. https://doi.org/10.1080/09593330.2018.1442880.

Wang, Z., Lu, Q., Liu, C., Tian, H., Wang, J., Xie, L., Liu, Q., Zeng, H., 2024. Nanoscale insights into the interaction mechanism underlying the adsorption and retention of heavy metal ions by humic acid. Environ. Sci. Technol. 58 (7), 3412. https://doi.org/10.1021/acs.est.3c08309.

Wojcieszyńska, D., Guzik, U., 2020. Naproxen in the environment: its occurrence, toxicity to nontarget organisms and biodegradation. Appl. Microbiol. Biotechnol. 104, 1849. https://doi.org/10.1007/s00253-019-10343-x.

Xiao, K., Horn, H., Abbt-Braun, G., 2022. "Humic substances" measurement in sludge dissolved organic matter: a critical assessment of current methods. Chemosphere 293, 133608. https://doi.org/10.1016/j.chemosphere.2022.133608.

Ye, Y., Cai, X., Wang, Z., Xie, X., 2022. Characterization of dissolved Black carbon and its binding behaviors to ceftazidime and diclofenac pharmaceuticals: employing the molecular weight fractionation. Environ. Pollut. 315, 120449. https://doi.org/10.1016/j.envpol.2022.120449.

Yuan, X., Yang, S., Fang, J., Wang, X., Ma, H., Wang, Z., Wang, R., Zhao, Y., 2018. Interaction mechanism between antibiotics and humic acid by UV-Vis spectrometry. Int. J. Environ. Res. Publ. Health 15, 1911. https://doi.org/10.3390/ijerph15091911.

Zheng, X., Xu, Z., Liu, J., 2022. Multiple roles of dissolved organic matter on typical engineered nanomaterials: environmental behaviours, pollutants removal and potential risks. Carbon Res. 1, 27. https://doi.org/10.1007/s44246-022-00026-0.

Zhou, Y., Zhang, Y., Li, P., Li, G., Jiang, T., 2014. Comparative study on the adsorption interactions of humic acid onto natural magnetite, hematite and quartz: effect of initial HA concentration. Powder Technol. 251, 1. https://doi.org/10.1016/j.powtec.2013.10.011.